UC Riverside

UC Riverside Previously Published Works

Title

Beneficial effects of sound exposure on auditory cortex development in a mouse model of Fragile X Syndrome

Permalink

https://escholarship.org/uc/item/0px6x0wk

Authors

Kulinich, Anna O
Reinhard, Sarah M
Rais, Maham
et al.

Publication Date

2020-02-01

DOI

10.1016/j.nbd.2019.104622

Peer reviewed

eScholarship.org Powered by the California Digital Library
University of California

*Manuscript
Click here to view linked References

Beneficial effects of sound exposure on auditory cortex development in a mouse model of Fragile X Syndrome

Running Title: **Effects of sound in Fragile X Syndrome**

Anna O Kulinich[1#], Sarah M Reinhard[2#], Maham Rais[1,4], Jonathan W Lovelace[2], Veronica Scott[1], Devin K Binder[1,3,4], Khaleel A Razak[2,3,4]*, Iryna M Ethell[1,3,4]*.

[1]*Division of Biomedical Sciences, School of Medicine, University of California, Riverside, CA, USA*
[2]*Psychology Department, University of California, Riverside, CA, USA*
[3]*Neuroscience Graduate Program, University of California, Riverside, CA, USA*
[4]*Biomedical Sciences Graduate Program, University of California, Riverside, CA, USA*

[#] These authors contributed equally

*Co-Corresponding Authors:

Iryna M. Ethell, PhD
Division of Biomedical Sciences
Email: iryna.ethell@medsch.ucr.edu
Phone: 951-827-2186

Khaleel A. Razak, PhD
Department of Psychology
Email: Khaleel@ucr.edu
Phone: 951-827-5060

Key words: Fragile X Syndrome, autism, auditory cortex, parvalbumin interneurons, perineuronal nets, sensory hypersensitivity

Abstract

Background

Fragile X syndrome (FXS) is the most common genetic cause of autism and intellectual disability. *Fragile X mental retardation gene* (*Fmr1)* knock-out (KO) mice display core deficits

of FXS, including abnormally increased sound-evoked responses, and show a delayed development of parvalbumin (PV) cells. Here, we present the surprising result that sound exposure during early development reduces correlates of auditory hypersensitivity in *Fmr1* KO mice.

Methods

Fmr1 KO and wild-type (WT) mice were raised in a sound-attenuated environment (AE) or sound-exposed (SE) to 14 kHz tones (5 Hz repetition rate) from P9 until P21. At P21-P23, event-related potentials (ERPs), dendritic spine density, PV expression and phosphorylation of tropomyosin receptor kinase B (TrkB) were analyzed in the auditory cortex of AE and SE mice.

Results

Enhanced N1 amplitude of ERPs, impaired PV cell development, and increased spine density in layers (L) 2/3 and L5/6 excitatory neurons were observed in AE *Fmr1* KO compared to WT mice. In contrast, developmental sound exposure normalized ERP N1 amplitude, density of PV cells and dendritic spines in SE *Fmr1* KO mice. Finally, TrkB phosphorylation was reduced in AE *Fmr1* KO, but was enhanced in SE *Fmr1* KO mice, suggesting that BDNF-TrkB signaling may be regulated by sound exposure to influence PV cell development.

Conclusions

Our results demonstrate that sound exposure, but not attenuation, during early developmental window restores molecular, cellular and functional properties in the auditory cortex of *Fmr1* KO mice, and suggest this approach as a potential treatment for sensory phenotypes in FXS.

Introduction

Auditory hypersensitivity is commonly associated with Autistic Spectrum Disorders (ASDs) and when present early in development can impede cognitive development, which relies on human interactions with the outside world through sensory inputs (Kern et al., 2006; Marco et al., 2011; Horder et al., 2014). While sound attenuation was beneficial in controlling behavior problems related to hyper-reactivity to sound in children with ASD (Ikuta et al., 2016), habitual use of sound attenuating devices may affect linguistic communication and result in exacerbation of sound sensitivity over time (Jastreboff and Hazell, 2008; Morris, 2009). Indeed, developmental reduction of auditory input can affect inhibitory synapses in auditory cortex (Takesian et al., 2012) and impair BDNF-dependent long-lasting inhibitory potentiation (Xu et al., 2010). Modulation of GABAergic circuits during development can result in long-lasting reversal of synaptic deficits following hearing loss in development (Kotak et al., 2013).

Fragile X syndrome (FXS) is a leading known genetic cause of autism (Harris et al., 2008) with symptoms that include intellectual disability, delayed language, social communication deficits, anxiety, seizures and sensory abnormalities (Rogers et al., 2001; Darnell and Klann, 2013), including auditory hypersensitivity (Rotschafer and Razak, 2013; Sinclair et al., 2017) and abnormal sensorimotor gating (Frankland et al., 2004). Enhanced N1 amplitude of auditory event-related potentials (ERPs; (Castren et al., 2003; Van der Molen et al., 2012)), impaired network synchronization (Ethridge et al., 2017) and altered brain responses to stimulus repetition (Schneider et al., 2013; Knoth et al., 2018) were also observed in FXS. FXS arises from a mutation in *fragile X mental retardation 1 gene* (*Fmr1*; (Liu et al., 2018) leading to its epigenetic silencing (Mor-Shaked and Eiges, 2018), a loss of FMR protein (FMRP; (Pieretti et

al., 1991)) and impaired FMRP-dependent protein translation (Darnell et al., 2011; Ferron, 2016), contributing to altered neuronal development and functions (Contractor et al., 2015).

Fmr1 knock out (KO) mouse model of FXS recapitulates many features of FXS pathophysiology (Kazdoba et al., 2014), including an increased density of immature dendritic spines (Rudelli et al., 1985; Irwin et al., 2001), elevated auditory cortical responses (Rotschafer and Razak, 2013; Wen et al., 2018), reduced habituation of ERP to auditory stimuli (Lovelace et al., 2016; Wen et al., 2018), increased EEG gamma band power (Lovelace et al., 2018; Wen et al., 2019), abnormal sensorimotor gating (Olmos-Serrano et al., 2011; Kokash et al., 2019), audiogenic seizures (Musumeci et al., 2000) and impaired auditory experience-dependent plasticity (Kim et al., 2013). Our previous studies suggest a novel cellular mechanism for auditory hypersensitivity in *Fmr1* KO mice, showing delayed development of parvalbumin (PV) cells and perineuronal nets (PNN), which often enwrap PV cells and regulate their excitability (Balmer, 2016). Neurons in the auditory cortex of *Fmr1* KO mice develop hyper-responsiveness during P14-P21 window (Wen et al., 2018), when their synaptic and intrinsic properties mature (Oswald and Reyes, 2008, 2011), coinciding with the critical period plasticity window (CPP) in the mouse auditory cortex (Kim et al., 2013). These studies suggest that cortical responses in *Fmr1* KO mice become abnormal within 10-12 days of hearing onset and may be driven by abnormal sensitivity to auditory input.

The purpose of this study was to examine the effects of sound-attenuated environment (AE) or passive sound exposure (SE) during early postnatal developmental period (P9-P21). We found reduced density of PV cells, increased dendritic spine density and larger N1 amplitude of ERPs in the auditory cortex of AE *Fmr1* KO mice to their (wild-type) WT counterparts. In contrast, exposing *Fmr1* KO mice to trains of pure 14 kHz tones during P9-P21 period

significantly increased the number of PV cells, normalized dendritic spine density and restored N1 response amplitude to WT levels.

Materials and methods

Ethics statement

All experiments and animal care/use protocols were approved by the Institutional Animal Care and Use Committee at the University of California, Riverside and were carried out in acccordance with NIH "Guide for the Care and Use of Laboratory Animals".

Mice and sound exposure

The FVB.129P2-Fmr1^{tm1Cgr}/J (*Fmr1* KO) and their control strain FVB.129P2-Pde6b^{+}Tyr$^{c\text{-}ch}$/AntJ (wild-type, WT) were originally obtained from the Jackson Laboratories (Sacramento, CA, USA). Animals were maintained in an AAALAC accredited facility under a 12-h light/dark cycle with water and food provided *ad libitum*. For the normal exposure (NE) group, mice were raised in an accredited vivarium from birth to the day of experiment (background ~65-70 dB SPL; BK Precision, model 732A). For the sound attenuated exposure (AE), age matched WT and *Fmr1* KO mouse litters with their mothers were housed together in a custom-built sound-shielded chamber lined with anechoic foam (105 cm x 105 cm x 63 cm, background ~37-40 dB SPL; BK Precision, model 732A sound level meter) from P4-7 until the time of testing (P20-P22). The chamber was placed in a room (275 cm x 420 cm) with background ~45 dB SPL, which was accessed only once daily for animal health checks. Although we used different litters of WT and Fmr1 KO mice, both WT and KO mice were reared together in the same chamber at the same time. In the sound exposure (SE) group, age matched WT and *Fmr1* KO mouse litters were

placed together in the same sound-shielded chamber and room with their mothers at P4-7 and exposed to pure tone pips (65 dB SPL; 14 kHz; 30 ms duration, 5 ms on/off ramp; 6 pips at a 5 Hz rep. rate; 2 s ITI) for 24h/day from P9 to P21. The sound was generated (Avisoft-SASlab Pro) and delivered through a speaker (Ultra Sound Gate Player BL Light; RECORDER USGH) placed in the center of the chamber mounted to the ceiling (~ 30 cm above the floor). No harmonics were detected during the sound delivery (Sokolich Probe Microphone System; Spectra DAQ-200). To prevent any tone exposure of the AE group, SE and AE groups did not temporally overlap and only one sound attenuation chamber was present in the room. Therefore, different WT and *Fmr1* KO mouse litters were used for SE versus AE experiment.

Immunofluorescence

Male WT and *Fmr1* KO mice were euthanized with isoflurane at P21-22 and perfused transcardially first with cold phosphate-buffered saline (PBS, 0.1 M) and then with 4% paraformaldehyde (PFA) in PBS. Brains were removed, post-fixed for 2 h in 4% PFA and 100 μm coronal sections containing auditory cortex were obtained using a vibratome (Campden Instruments) with a speed of 0.5-0.65 mm/s. Identification of auditory cortex was performed using hippocampal landmarks (Wen et al., 2018). This method was previously validated using tonotopic mapping, dye injection (Martin del Campo et al., 2012) and Paxinos mouse brain atlas and other publications on mouse auditory cortex (Anderson et al., 2009).

On average, 5–6 slices containing auditory cortex were obtained from each brain. Immunolabeling of sections was performed using the following protocol. Brain slices were post-fixed with 4% PFA in 0.1 M PBS for an extra 2 h and then washed in 0.1 M PBS. Then, brain tissues were incubated with 50 mM ammonium chloride for 15 minutes to quench residual PFA

and washed with PBS. Next, 0.1% Triton X-100 in PBS was applied to permeabilize slices, which was followed by incubation in 5% Normal Goat Serum (NGS; Sigma, catalog# G9023-10 mL) and 1% Bovine Serum Albumin (BSA; Fisher Scientific, catalog# 9 048468) in 0.1 M PBS solution to block tissue nonspecific staining. Sections were further incubated with primary antibodies and fluorescein-tagged *Wisteria floribunda* agglutinin (WFA, 4 µg/mL; Vector Laboratories, cat# FL-1351, RRID:AB_2336875) in 0.1 M PBS containing 1% NGS, 0.5% BSA, and 0.1% Tween-20 for 24 h. Mouse anti-PV antibody (1:1000; Sigma, catalog# P3088, RRID:AB_477329) was used to visualize PV+ interneurons. WFA, a lectin that recognizes glycosaminoglycan side chains of chondroitin sulfate proteoglycans present in PNNs, primarily but not exclusivley aggrecan, was used to label PNNs, referred here as WFA+ PNNs (Pizzorusso et al., 2002). Next, slices were washed in 0.1 M PBS containing 0.5% Tween-20 and incubated with secondary antibodies, donkey anti-mouse Alexa 594 (4 µg/mL; Thermo Fisher Scientific, catalog# A-21203, RRID:AB_2535789), in 0.1 M PBS for 1 h. Brain tissues were further washed with 0.1 M PBS containing 0.5% Tween-20, mounted with Vectashield (Vector Labs, catalog# H-1200) and sealed with Cytoseal (ThermoScientific, catalog# 8310–16). Each slice was imaged with a Leica TCS SP5 confocal microscope using a series of 10 high-resolution optical sections (1024 × 1024-pixel format) and a 10×, or a 63× water-immersion objective (1.2 numerical aperture), 1× zoom at 1µm step (z-stack). For the analysis, each z-stack was collapsed into a single image, converted to a TIFF file using Image J and encoded for blind analysis. Image J was also used to analyze density of PNN+cells, PV+ cells and their colocalization in cortical layers 2-6. T-test was used to determine genotype specific differences for each experiment. Statistical analyses were performed using Microsoft Excel and GraphPad Prism 7.

Dendritic spine labeling and analysis

Brain slices were collected as described above and dendritic spines were labeled using DiO-listic approach as previously described (Staffend and Meisel, 2011). Tungsten particles were coated with 1,1′-dioctadecyl-3,3,3′,3′-tetramethylindocarbocyanine perchlorate (DiI; catalog# D282, Invitrogen), delivered to the brain slices by helium-powered ejection (Bio-Rad Helios Gen Gun System) and further incubated in PBS for 72 h at 4°C before being mounted onto slides in PBS and sealed with Cytoseal (ThermoScientific, catalog# 8310–16). Labeled neurons were first identified in layers (L) 1-6 of auditory cortex using confocal microscopy with 10× objective (model LSM 510, Carl Zeiss MicroImaging) and images of basolateral dendrites of L2-6 neurons in respective layers were captured with a 63× water-immersion objective (1.2 numerical aperture) and 1× zoom using a series of high-resolution optical sections (1024 × 1024-pixel format) at 0.5 μm step intervals (*z*-stack). Each *z*-stack was collapsed into a single image by projection (LSM Image Browser, Zeiss), converted to a TIFF file and encoded for blind analysis. Analysis of the spine density (spines per 10 μm dendrite) and volume (μm^3) was performed using Neurolucida 360 software (MicroBrightField; RRID: SCR_001775) (Koeppen et al., 2018). At least five animals (AE WT, n=5; AE *Fmr1* KO, n=7; SE WT, n=5; SE *Fmr1* KO, n=7) were analyzed per group, and dendrites from at least 5 neurons were imaged per animal (AE WT, n=33; AE *Fmr1* KO, n=39; SE WT, n=28; AE *Fmr1* KO, n=38).

Electrophysiology

Auditory ERPs were recorded to quantify P1, N1, P2 amplitudes and latencies across the different groups of mice. Mice were anesthetized with ketamine-xylazine (K/X) (80/10 mg/kg) with half dose supplements as needed. They were secured on a bite bar, and placed on a

stereotaxic apparatus (model 930; Kopf, CA). To monitor the anesthetic state, a toe pinch reflex was assessed every 20–30 min throughout the experiment. Once the animal was anesthetized, a midline sagittal incision along the scalp was made to expose the skull, and the right temporalis muscle was displaced. A dental drill was used to remove the skull over the right auditory cortex (Martin del Campo et al., 2012). Location of core auditory cortex was identified using vasculature, and confirmed with extracellular local field potential recordings using broadband sound (0.25 Hz repetition rate) and a tungsten microelectrode (FHC Inc., diameter 125 µm). At the end of the experiment, mice were euthanized with sodium pentobarbital (i.p. 125 mg/kg).

ERP recordings were obtained in a sound-attenuated chamber lined with anechoic foam (Gretch-Ken Industries, Oregon) as previously described (Lovelace et al., 2016). Acoustic stimuli were generated using TDT RZ6 system and presented through a free-field speaker (LCY-K100 ribbon tweeters; Madisound, WI) located 6 in. away at a 45° angle from the animal's left ear. Sound level was modified using programmable attenuators (PA5; Tucker-Davis Technologies, Florida). The speaker output was flat within +/− 3 dB for frequencies between 5 and 35 kHz as measured using a 1/4 inch B&K microphone. The stimulus consisted of trains of 10 repeating pure tones (14 kHz or 23 kHz, 100 ms duration), 5 ms rise/fall time, 8 s inter-train interval 70 dB SPL presented at 0.25 Hz repetition rate. After 5 min of baseline recordings with no auditory stimulation, at least 50 repetitions (5 trains with 10 tone pips each) of the tone was presented. Auditory ERP recordings were obtained using the BioPac system (BIOPAC Systems, Inc.). A tungsten microelectrode (FHC Inc.) was advanced into the brain using a Kopf direct drive 2660 micropositioner (depth 350-600 µm). A stainless steel wire (California Fine Wire Company) was attached to the neck muscle for grounding purposes. At each recording location, testing began only after sound-driven ERPs with an N1 component with ~30-80 ms latency could

be reliably produced. The BioPac MP150 acquisition system was connected to an EEG 100C amplifier unit to which the recording electrode and ground were attached. Signals were filtered (high-pass (0.5 Hz) and low-pass (35 Hz)). Data were sampled at a rate of either 5 or 20 kHz using Acqknowledge software, and sound delivery was synchronized with ERP recording using a 5 ms digital TTL pulse to mark the onset of each sound in a train. ERP traces were extracted from Acknowledge and converted to files compatible with Brain Vision Analyzer 2.1. Artifact rejection was done using several criteria such as amplitude, gradient, max-min and low activity. After that, recorded traces were subdivided into 250 ms segments based on a TTL pulse that marked the sound stimulus onset. P1, N1 and P2 were detected based on maximal positive or negative deflections in a certain time window: P1 (10-50 ms), N1 (30-80 ms) and P2 (75-150 ms).

Western blotting

Mice were euthanized at P21 with isoflurane and cervical dislocation was performed. Auditory cortex was identified based on methods described earlier and dissected. Tissue samples were immediately homogenized in cold HEPES buffer (4 mM HEPES buffer, pH 7.5; 300 mM sucrose; 150 mM NaCl; 0.1 mM phenylmethylsulfonyl fluoride (PMSF); protease inhibitor cocktail (Sigma, P8340); 0.5 mM sodium orthovanadate) to extract soluble cytoplasmic proteins for PV detection. Another subset of tissue samples were collected and lysed in RIPA buffer (50 mM Tris-HCl, pH 7.4; 150 mM NaCl; 1 mM EDTA, pH 8.0; 1% Triton X-100; 0.1% SDS; protease inhibitor cocktail; 0.5 mM sodium pervanadate) to extract membrane-bound proteins for detection of tropomyosin kinase B (TrkB). In both cases, samples were rotated at 4°C for 1 h to allow for complete cell lysis and then cleared by centrifugation at 13,200 rpm for 20 min at 4°C.

Samples were boiled in reducing sample buffer (Laemmli 2× concentrate, S3401, Sigma), and separated on 8–16% Tris-glycine SDS-PAGE precast gels (Invitrogen). Proteins were transferred onto Protran BA 85 Nitrocellulose membrane (GE Healthcare), washed 2 times (5 min each) with miliQ water and further blocked for 1 h at room temperature in 5% BSA (BSA; Fisher Scientific, catalog# 9048468) or skim milk (catalog #170-6404, Bio-Rad), based on the manufacture's staining protocol. Incubation with primary antibody diluted in TBS/0.1% Tween-20/5% BSA was performed overnight at 4°C. The following primary antibodies for protein detection were used: mouse anti-PV (1:1000; Millipore, catalog# MAB1572, RRID:AB_ 2174013), rabbit anti-β-actin (1:2000; Abcam, catalog# Ab8227, RRID:AB_2305186), mouse anti-total TrkB (1:2000; BD Transduction Laboratories, catalog# 610101, RRID:AB_AB_397507), rabbit anti-phospho-TrkB (Tyr816) (1:2000; Millipore, catalog# ABN1381, RRID:AB_2721199)) and rabbit anti-phospho-TrkB (Tyr515) (1:1000; Bioworld, catalog# AP0236). Blots were washed 3 × 10 min with TBS/0.1% Tween-20 and incubated with the appropriate HRP-conjugated secondary antibodies for 1 h at room temperature in a TBS/0.1% Tween-20/5% BSA solution. The secondary antibodies used were α-rabbit-HRP (Thermo Fisher Scientific, catalog #G-21234, RRID: AB_2536530) at 1:10000 and α-mouse-HRP at 1:10000 (Jackson ImmunoResearch Labs, catalog #715-035-150, RRID:AB_2340770). Next, blots were washed 3 × 10 min in TBS/0.1% Tween-20 and 1× 10 min TBS and developed with ECL Detection reagent (catalog# 80196, Thermo Scientific). For reprobing, membrane blots were washed in stripping buffer (2% SDS, 100 mM β-mercaptoethanol, 50 mM Tris-HCl, pH 6.8) for 30 min at 55°C, then rinsed repeatedly with TBS/0.1% Tween-20 (5×5 min), blocked with 5% skim milk, and then reprobed. X-ray film (Thermo Scientific) was used for the protein bands signal detection, which was further processed using mini-medical X-ray processor (AFP

Imaging). Developed films were then scanned, and band density was analyzed by measuring band and background intensity using Adobe Photoshop CS5.1 software (RRID:SCR_014199). Samples from *Fmr1* KO and their counterpart WT mice (NE, AE or SE groups) were run on the same blot, and precision/tolerance (P/T) ratios for *Fmr1* KO samples were normalized to averaged P/T ratios of WT samples.

Data analysis

Statistical analysis was performed using unpaired t-test to determine genotype differences within the same sound exposure group (NE WT vs NE *Fmr1* KO, AE WT vs AE *Fmr1* KO or SE WT vs SE *Fmr1* KO). In order to compare the effect of sound exposure, two-way ANOVA was performed (sound exposure, genotype) followed by Bonferroni's post hoc pair-by-pair comparisons between AE and SE groups. In all cases, GraphPad Prism 7 was used for the analysis and data represent mean ± standard error of the mean (SEM).

Results

AE *Fmr1* KO mice show enhanced auditory ERP NI amplitudes

Tone-evoked single unit responses are increased in auditory cortex of P21 *Fmr1* KO mice compared to WT mice (Wen et al., 2018). These mice were raised in a regular vivarium with a variety of environmental sounds (NE group). We hypothesized that developmental attenuation of environmental sounds might normalize cortical development. To test this hypothesis, we raised mice in a sound-attenuating box (AE) with the background noise averaging ~37-40 dB SPL (compared ~65-70 dB SPL in the vivarium) during early postnatal P9-P21 period. We next recorded ERPs from auditory cortex of P21-P23 mice in response to 14 kHz or 23 kHz tones and

measured peak amplitudes and latencies of P1, N1 and P2 components (Fig.1A-H, Fig.S1A-F). 14 kHz and 23 kHz were chosen based on previously published results, which demonstrate that higher percentage of cortical neurons respond to 11-15 kHz tones compared to 21-25 kHz (Rotschafer and Razak, 2013). The P1 and P2 amplitudes evoked by 14 kHz and 23 kHz tones were not significantly different between AE WT and AE *Fmr1* KO mice (Fig.1A-C, 1E-F, 1H). However, higher N1 amplitude was detected in response to 14 kHz tone ($p=0.0496$; Fig. 1A, D; Table S1), but not to 23 kHz tone (Fig.1B, 1G; Table S2), in AE *Fmr1* KO compared to AE WT mice.

No significant differences were detected in P1 and N1 latencies in response to 14 kHz and 23 kHz between AE *Fmr1* KO and WT mice (Fig.S1A, B, D, E; Table S1-S2), whereas a longer P2 latency was found in AE *Fmr1* KO mice compared to AE WT in response to 14 kHz ($p=0.0093$; Fig.S1C) but not 23 kHz (Fig.S1F; Table S1-S2).

In summary, enhanced responses were observed in P21-P23 auditory cortex of *Fmr1* KO mice raised in sound-attenuated environment compared to their WT counterparts, similar to our previous findings in *Fmr1* KO mice raised in the standard vivarium.

SE *Fmr1* KO mice exposed to 14 kHz tone during development exhibit normal sound-evoked responses

We next tested whether passive developmental sound exposure of mice would normalize sound-evoked responses in *Fmr1* KO mice. Because we observed a difference in N1 amplitude between AE *Fmr1* KO and AE WT in response to 14 kHz tone, we chose this frequency for exposure with ~65dB SPL (de Villers-Sidani et al., 2008; Kim et al., 2013; Zhu et al., 2014). WT

and *Fmr1* KO mice were placed in a sound-attenuated chamber at P5 and exposed to 14 kHz tone pip trains 24 h/day from P9 to P21-23 when analysis was performed.

Analysis of average peak amplitude and latency of raw ERP P1, N1 and P2 components in auditory cortex of SE WT and SE *Fmr1* KO mice showed no genotype differences for both 14 kHz and 23 kHz tones (Fig.2A-H; Fig.S1G-L, Table S1-S2). Specifically, N1 peak amplitude evoked by 14 kHz tone in SE *Fmr1* KO mice was not significantly different from SE WT group (Fig.2D). Interestingly, two-way ANOVA analysis of P1, N1 or P2 latencies evoked by 14 kHz with exposure (AE, SE) and genotype (WT, *Fmr1* KO) as factors showed exposure effect (P1: $F_{(1.53)}$=4.101, p=0.0479; N1: $F_{(1,53)}$=6.369, p=0.0146; P2: $F_{(1,53)}$=7.626, p=0.0079) and interaction (N1: $F_{(1.53)}$=5.502, p=0.0228; P2: $F_{(1,53)}$=7.609, p=0.0080) with significant differences between SE *Fmr1* KO mice and AE *Fmr1* KO mice with Bonferroni's multiple comparisons test (P1: p=0.0148; N1: p=0.0012, P2: p=0.0002). Further, two-way ANOVA analysis of P1, N1 or P2 latencies evoked by 23 kHz with exposure (AE, SE) and genotype (WT, *Fmr1* KO) as factors also showed exposure effect (N1: $F_{(1.52)}$=6.096, p=0.0169; P2: $F_{(1,52)}$=12.15, p=0.0010) with significant differences between SE *Fmr1* KO mice and AE *Fmr1* KO mice with Bonferroni's multiple comparisons test (P1: p=0.0246; N1: p=0.0071; P2: p=0.0007). No differences in P1, N1 and P2 amplitudes and latencies were observed between SE WT and AE WT mice (Fig.S1G-L).

Our results show that developmental sound exposure restored sound evoked N1 amplitude and P2 latency in auditory cortex of *Fmr1* KO mice to WT levels.

Developmental exposure of SE *Fmr1* KO mice to 14 kHz tone reverses impaired development of PV cells in the auditory cortex of AE *Fmr1* KO mice

A reduced density of PV interneurons and PNNs were previously demonstrated in the auditory cortex of P21 *Fmr1* KO compared to WT mice, which may underlie abnormal responses to sound (Wen et al., 2018). Here we examined the density of PV+ interneurons and PNNs in the auditory cortex of AE and SE *Fmr1* KO mice at P21 (Fig.3A-O).

We found that PV cell density was significantly reduced in L2/3 ($p<0.0001$; Fig.3D) and L4 ($p<0.0001$; Fig.3G) of AE *Fmr1* KO compared to AE WT mice. Similar changes were observed in L5/6 (Table S3). We also observed decreased density of PNNs in L4 ($p=0.0025$; Fig.3H) and L5/6 ($p=0.0240$; Table S3) in *Fmr1* KO compared to WT mice. No differences in PNN density were observed in L2/3 *Fmr1* KO and WT mice (Fig.3E), likely due to low density of PNNs in L2/3. Analysis of PV and PNN co-localization showed lower density of PV cells with PNN in L4 ($p=0.0031$; Fig.3I) and L5/6 ($p=0.0140$; Table S3) in *Fmr1* KO compared to WT mice. Interestingly, we also observed a reduction in the density of PV cells lacking PNNs in L2/3 ($p<0.0001$; Table S3), L4 ($p=0.0024$; Table S3) and L5/6 ($p=0.0001$; Table S3) in *Fmr1* KO compared to WT mice, which was not previously reported in NE mice (Wen et al., 2018). Thus, auditory cortex of *Fmr1* KO mice raised in sound-attenuated environment exhibit a decreased density of PV cells and PNNs compared to sound-attenuated WT counterparts, as previously seen in *Fmr1* KO mice raised in the standard vivarium.

In contrast, PV cell density in SE *Fmr1* KO was similar to SE WT level (Fig.3J, 3M; Table S3), suggesting that the sound exposure restored PV cell development to normal levels in *Fmr1* KO mice. However, density of PNNs remained lower in L4 auditory cortex of SE *Fmr1* KO as compared to SE WT mice ($p=0.0026$; Fig.3N), but no differences were observed between SE *Fmr1* KO and SE WT mice in L5/6 ($p=0.56$; Table S3). The density of PV cells containing PNNs was also not significantly different between SE WT and SE *Fmr1* KO mice (Fig.3L, 3O).

A two-way ANOVA analysis was used to compare SE and AE groups that were raised in the same chamber with (SE) or without (AE) sound exposure. The analysis with exposure (AE, SE) and genotype (WT, *Fmr1* KO) as factors showed no exposure effect ($F_{(1,23)}$=3.655, p=0.0685), but showed a significant genotype effect ($F_{(1,23)}$=23.44, p<0.0001) and interaction ($F_{(1,23)}$=5.549, p=0.0274). However, pairwise comparison with Bonferroni's multiple comparisons test revealed an increased PV cell density in SE *Fmr1* KO compared to AE *Fmr1* KO (p<0.05), but no difference between SE WT and AE WT (p>0.9999) in all layers.

Taken together, the results demonstrate that exposing mice to 14 kHz tone during development results in increased density of PV cells in all layers of *Fmr1* KO mice to WT levels, without affects on PNNs.

AE but not SE *Fmr1* KO mice auditory cortex neurons show abnormal increase in dendritic spine density

Dendritic spine density and morphology were analyzed in L2-6 auditory cortex of AE and SE mice using DiOlistic approach (Fig.4A-L). A significantly higher dendritic spine density was observed in basolateral dendrites of L2/3 and L5/6 excitatory neurons in AE *Fmr1* KO compared to WT mice (p=0.0061, Fig.4E; p=0.0090, Fig.4I), but L4 neurons were not different (Table S4). Dendritic spine morphology was evaluated based on spine volume, where spines with small volume (less than 0.5 μm^3) represent immature spines with small heads and spines with large volume represent mature spines (stubby- or mushroom-like spines with large heads (Koeppen et al., 2018). No differences in spine morphology were detected in L2/3 and L5/6 auditory cortex between WT and *Fmr1* KO (Fig.4F, 4J). Thus, *Fmr1* KO mice raised in sound-attenuated

environment show increased spine density in L2/3 and L5/6 neurons, but no significant changes in dendritic spine morphology.

In contrast, dendritic spine density in basolateral dendrites of L2/3 and L5/6 excitatory neurons was similar in SE *Fmr1* KO and WT mice (Fig.4C-D, 4G-H, 4K-L; Table S4). There was one significant difference in spine morphology detected in L2/3 auditory cortex of SE *Fmr1* KO compared SE WT mice, showing a decrease in the proportion of large spines ($p<0.05$; Fig.4H). A two-way ANOVA with exposure (AE, SE) and genotype (WT, *Fmr1* KO) as factors showed an effect of sound exposure on spine density in L2/3 auditory cortex ($F_{(1,122)}=35.47$, $p<0.0001$) with significant changes in both WT (AE WT vs SE WT, $p=0.0011$) and *Fmr1* KO mice (AE *Fmr1* KO vs SE *Fmr1* KO, $p<0.0001$) with Bonferroni's multiple comparisons test. In L5/6, there was only a significant effect of sound exposure in *Fmr1* KO (AE *Fmr1* KO vs SE *Fmr1* KO, $p=0.0006$, Bonferroni's multiple comparisons test).

In summary, developmental sound exposure restored dendritic spine density in auditory cortex of *Fmr1* KO mice to WT levels.

SE *Fmr1* KO mouse auditory cortex shows normal PV protein levels and increased TrkB phosphorylation

To assess whether the reduction in the density of PV cells in the auditory cortex of AE *Fmr1* KO mice is a result of reduced PV levels, we examined PV protein levels in the auditory cortex using Western blotting. While there was no difference in PV levels between NE *Fmr1* KO and WT (Fig.5A), PV levels were significantly decreased in AE *Fmr1* KO mice compared to AE WT ($p=0.0403$; Fig.5B). In contrast, SE *Fmr1* KO mice showed similar PV levels as SE WT (Fig.5C; Table S5).

As TrkB signaling is implicated in PV cell development and survival (Nomura et al., 2017; Xenos et al., 2018) we also evaluated total and phosphorylated levels of TrkB in WT and *Fmr1* KO mice. We found that TrkB levels (145 kDa) were similar between *Fmr1* KO and WT in all groups (Fig.5D-F). We further examined activation of TrkB by evaluating its phosphorylation (p) on the tyrosine (Y)816 and Y515. No differences in pTrkB-Y816 and pTrkB-Y515 were observed in NE *Fmr1* KO compared to NE WT (Fig.5G, 5J). However, we observed a significant decrease in pTrkB-Y816 and pTrkB-Y515 in AE *Fmr1* KO compared to AE WT (pY816: p=0.0479 and pY515: p=0.0306; Fig.5H, 5K). Interestingly, a significant increase in pTrkB-Y515, but not pTrkB-Y816, levels was observed in SE *Fmr1* KO mice compared to SE WT (p=0.0004; Fig.5I, 5L, Table S5). A two-way ANOVA analysis with exposure (AE, SE) and genotype (WT, *Fmr1* KO) as factors showed the effect of sound exposure on both pTrkB-Y816 (exposure effect: $F_{(2,34)}$=4.005, p=0.0274 and interaction effect: $F_{(2.34)}$=4.023, p=0.0270) and pTrkB-Y515 levels (exposure effect: $F_{(2,34)}$=7.415, p=0.0021 and interaction effect: $F_{(2,34)}$=7.427, p=0.0021). Pairwise comparison with Bonferroni's multiple comparisons test revealed an increase of pTrkB-Y816 levels (p=0.0015) and pTrkB-Y515 levels (p<0.0001) in SE *Fmr1* KO compared to AE *Fmr1* KO. This parallels the increased PV cell density we observed in SE *Fmr1* KO mice.

Together, our results indicate that developmental sound exposure increased PV level and TrkB phosphorylation in auditory cortex of *Fmr1* KO mice.

Discussion

We demonstrate differential effects of auditory experience on auditory cortex development in WT and *Fmr1* KO mice. First, we found enhanced sound-evoked responses in

Fmr1 KO mice compared to WT mice raised in sound-attenuated environment that are associated with increased dendritic spine density, but reduced PV expression and TrkB phosphorylation. This suggests that developmental sound attenuation may not be feasible to reduce auditory hypersensitivity in FXS. In contrast, we observed beneficial effects of developmental tone exposure in restoring molecular, cellular and functional properties in the auditory cortex of *Fmr1* KO mice to WT levels. Specifically, comparison of sound-exposed *Fmr1* KO mice to *Fmr1* KO mice reared in sound-attenuated environment show: (1) reduced N1 amplitude of ERPs; (2) increased PV expression; (3) decreased dendritic spine density; and (4) enhanced TrkB phosphorylation (Fig.6).

One major finding of this study is the modulation of PV cell density in auditory cortex of *Fmr1* KO following passive developmental sound exposure. PV cells are GABAergic interneurons that regulate network oscillations associated with sensory processing and contribute to the maintenance of E/I balance (Sohal et al., 2009; Hu and Jonas, 2014). Our previous work showed delayed PV cell development in the auditory cortex of *Fmr1* KO mice (Wen et al., 2018). This is consistent with studies of somatosensory and visual cortices of *Fmr1* KO mice, suggesting a common role of PV interneurons in abnormal sensory processing and hypersensitivity in FXS (Selby et al., 2007; Gibson et al., 2008; Goel et al., 2018). In this study, we found that developmental sound attenuation did not restore normal PV cell development, suggesting that sensory input is probably not the primary cause of the deficit in *Fmr1* KO mice. In contrast, developmental exposure to 14 kHz sound increased PV cell density and PV/PNN co-localization in auditory cortex of *Fmr1* KO mice. Given the consistent deficits in PV cell density and function across sensory systems, our data suggest the possibility of passive sound exposure during development as a potential approach to reduce hypersensitivity. However, SE *Fmr1* KO

mice still show impaired PNN formation in L4 auditory cortex suggesting possible benefits of combining pharmacological interventions to restore PNN levels and acoustic exposure during cortical development. Our previous studies implicated enhanced MMP-9 activity in impaired PNN formation and abnormal cortical responses in *Fmr1* KO mice (Sidhu et al., 2014; Wen et al., 2018). Genetic reduction of MMP-9 in *Fmr1* KO mice resulted in normal development of PNNs and normal response magnitudes in auditory cortical neurons (Wen et al., 2018), providing a justification for targeting MMP-9 pharmacologically. It is possible that enhanced MMP-9 activity may result in excessive cleavage of aggrecan and a reduction in aggrecan-containing PNNs detected with WFA (Roughley and Mort, 2014; Miyata and Kitagawa, 2016; Lovelace et al., 2019). Future studies will determine whether acute or chronic MMP-9 inhibition during development will restore PNN formation and normalize cortical responses in *Fmr1* KO mice.

Another finding of this study is that developmental sound exposure normalized density of dendritic spines, major postsynaptic sites of excitatory synapses, in auditory cortex of *Fmr1* KO mice. An abundance of immature dendritic spines is seen in the brains of humans with FXS (Irwin et al., 2001) and *Fmr1* KO mice (Comery et al., 1997). However, there are controversial results on spine density in developing and adult *Fmr1* KO that are influenced by mouse genetic background, brain area and developmental period (He and Portera-Cailliau, 2013). In this study, we demonstrate that developmental sound exposure reduces dendritic spine density on basolateral dendrites of L2/3 and L5/6 excitatory neurons in P21 *Fmr1* KO auditory cortex to WT levels. Our data show that the acoustic manipulations during early postnatal development influence developing synaptic circuits in *Fmr1* KO auditory cortex by affecting both inhibitory and excitatory neurons.

In AE *Fmr1* KO mice, decreased PV cell density and increased spine density is predicted to favor excitation over inhibition. Indeed, when ERPs were recorded from the auditory cortex, AE *Fmr1* KO mice showed larger N1 amplitudes in response to 14 kHz, but not 23 kHz, tone than their WT counterparts. Although a large number of adult auditory cortical neurons respond to frequencies ~20-25 kHz range (Zhou et al., 2008; Barkat et al., 2011; Carrasco et al., 2013), the tonotopic maps develop high frequency selectivity later in development (Zhang et al., 2001; Carrasco et al., 2013). Therefore, at P21 there may be more neurons responding to frequencies <20 kHz in the auditory cortex. Abnormal synchrony, which is a key feature in developing *Fmr1* KO mice (Goncalves et al., 2013), may be also responsible for a larger ERP evoked by the 14 kHz tone in *Fmr1* KO mice, compared to WT. This is consistent with larger tone-evoked ERP amplitudes in humans with FXS (Castren et al., 2003; Schneider et al., 2013; Knoth et al., 2018) and our previous studies showing enhanced auditory cortical single-unit responses and impaired habituation to repeated sounds in *Fmr1* KO mice (Rotschafer and Razak, 2013; Lovelace et al., 2016; Wen et al., 2018). Interestingly, developmental sound exposure resulted in a decrease of P1, N1 and P2 latencies of ERP evoked by both 14 kHz and 23 kHz tones in auditory cortex of SE *Fmr1* KO mice compared to AE *Fmr1* KO, which indicate maturation of these ERP components. (Kim et al., 2013) showed that exposure of mice to 16 kHz during development increased the tonotopic representation of 16 kHz in WT, but not in *Fmr1* KO mice, suggesting abnormal critical period plasticity in the *Fmr1* KO mice. This tonotopic plasticity is unlikely to contribute to our ERP findings as ERP amplitude was not different between SE WT and SE *Fmr1* KO mice in spite of larger 16 kHz representation observed previously in WT mice (Kim et al., 2013). We also observed a reduction of average ERP N1 amplitude in *Fmr1* KO mice following developmental exposure to sound without changes in the WT mice. Future

experiments should more closely explore relationships between tonotopic maps and ERPs in order to understand the underlying mechanisms. Taken together, our data suggest that passive exposure of mice to pure tones during the auditory critical period normalizes the cellular and functional properties of the auditory cortex in *Fmr1* KO mice.

While the observed increase in the density of PV cells may underlie the changes in auditory cortical responses of sound-exposed *Fmr1* KO mice, the mechanism of the up-regulation is still not clear. BDNF-TrkB signaling is implicated in the development and function of GABAergic neurons (Nakahara et al., 2004; Berghuis et al., 2006). TrkB signaling supports PV cells and influences gamma-band synchronization in hippocampus (Zheng et al., 2011; Lucas et al., 2014). In cortex, TrkB deletion from PV interneurons resulted in dysregulation of patterned high-frequency cortical activity and disinhibition of local excitatory neurons (Xenos et al., 2018). In *Fmr1* KO mice, BDNF-TrkB signaling was implicated in FXS-associated alterations (Castren and Castren, 2014). Impaired BDNF-TrkB signaling may cause delayed development of fast spiking interneurons in P5 *Fmr1* KO somatosensory cortex, which was restored following the administration of the TrkB agonist LM22A-4 (Nomura et al., 2017). In contrast, a reduced density of PV interneurons with increased TrkB expression was demonstrated in adult *Fmr1* KO mice (Selby et al., 2007). In our study, we did not observe changes in total TrkB levels, but TrkB phosphorylation on Y816 and Y515 was reduced in auditory cortex of AE *Fmr1* KO mice compared to AE WT. Interestingly TrkB phosphorylation was increased in *Fmr1* KO auditory cortex after sound exposure that was concurrent with the increase in PV expression, suggesting a role of TrkB signaling in regulating PV cells in the auditory cortex of sound-exposed *Fmr1* KO mice. Genetic reduction of BDNF levels in neural precursor cells derived from *Fmr1* KO mice increased pTrkB-Y816, but not pTrkB-Y515 levels, suggesting changes

that are compensatory to BDNF signaling deficit (Danesi et al., 2018). Interestingly, hyperactivity and deficits in startle responses were ameliorated in *Bdnf(+/-)/Fmr1* KO mice, suggesting a possible role of BDNF/trkB signaling in these behaviors (Uutela et al., 2012).

Conclusions

Alterations of the acoustic environment during early postnatal developmental window lead to changes of PV expression, spine density and auditory responses in *Fmr1* KO mice. Our data suggest that sensory manipulations during a critical developmental period might influence neuronal circuit development and E/I balance in FXS providing a basis for future studies of sensory manipulations in addition to pharmacological interventions. These results also make the intriguing suggestion that some deficits observed during early postnatal developmental period in *Fmr1* KO mouse auditory system may trigger compensatory mechanisms to restore responses (Antoine et al., 2019). More studies are necessary to investigate which parameters of the sound exposure are key to observed changes and to understand long-lasting effects of the early developmental exposure. In addition, our data suggest the need to perform high-resolution developmental studies to measure cellular and circuit changes across different brain areas with a stringent control of sensory input to understand the relative contributions of direct genetic effects and changes that arise due to altered experience.

Disclosures: We report no conflict of interest.

Acknowledgements: This work was supported by the US Army Medical Research grant W81XWH-15-1-0436. We thank members of Drs. Ethell, Razak, and Binder laboratories for

helpful discussions, comments and technical support; David Carter for advice on confocal microscopy.

References

Anderson LA, Christianson GB, Linden JF (2009) Mouse auditory cortex differs from visual and somatosensory cortices in the laminar distribution of cytochrome oxidase and acetylcholinesterase. Brain Res 1252:130-142.

Antoine MW, Langberg T, Schnepel P, Feldman DE (2019) Increased excitation-inhibition ratio stabilizes synapse and circuit excitability in four autism mouse models. Neuron 101:648-661 e644.

Balmer TS (2016) Perineuronal Nets Enhance the Excitability of Fast-Spiking Neurons. eNeuro 3.

Barkat TR, Polley DB, Hensch TK (2011) A critical period for auditory thalamocortical connectivity. Nat Neurosci 14:1189-1194.

Berghuis P, Agerman K, Dobszay MB, Minichiello L, Harkany T, Ernfors P (2006) Brain-derived neurotrophic factor selectively regulates dendritogenesis of parvalbumin-containing interneurons in the main olfactory bulb through the PLCgamma pathway. J Neurobiol 66:1437-1451.

Carrasco MM, Trujillo M, Razak K (2013) Development of response selectivity in the mouse auditory cortex. Hear Res 296:107-120.

Castren M, Paakkonen A, Tarkka IM, Ryynanen M, Partanen J (2003) Augmentation of auditory N1 in children with fragile X syndrome. Brain Topogr 15:165-171.

Castren ML, Castren E (2014) BDNF in fragile X syndrome. Neuropharmacology 76 Pt C:729-736.

Comery TA, Harris JB, Willems PJ, Oostra BA, Irwin SA, Weiler IJ, Greenough WT (1997) Abnormal dendritic spines in fragile X knockout mice: maturation and pruning deficits. Proc Natl Acad Sci U S A 94:5401-5404.

Contractor A, Klyachko VA, Portera-Cailliau C (2015) Altered neuronal and circuit excitability in fragile X syndrome. Neuron 87:699-715.

Danesi C, Achuta VS, Corcoran P, Peteri UK, Turconi G, Matsui N, Albayrak I, Rezov V, Isaksson A, Castren ML (2018) Increased calcium influx through L-type calcium channels in human and mouse neural progenitors lacking fragile X mental retardation protein. Stem Cell Reports.

Darnell JC, Klann E (2013) The translation of translational control by FMRP: therapeutic targets for FXS. Nat Neurosci 16:1530-1536.

Darnell JC, Van Driesche SJ, Zhang C, Hung KY, Mele A, Fraser CE, Stone EF, Chen C, Fak JJ, Chi SW, Licatalosi DD, Richter JD, Darnell RB (2011) FMRP stalls ribosomal translocation on mRNAs linked to synaptic function and autism. Cell 146:247-261.

de Villers-Sidani E, Simpson KL, Lu YF, Lin RC, Merzenich MM (2008) Manipulating critical period closure across different sectors of the primary auditory cortex. Nat Neurosci 11:957-965.

Ethridge LE, White SP, Mosconi MW, Wang J, Pedapati EV, Erickson CA, Byerly MJ, Sweeney JA (2017) Neural synchronization deficits linked to cortical hyper-excitability and auditory hypersensitivity in fragile X syndrome. Mol Autism 8:22.

Ferron L (2016) Fragile X mental retardation protein controls ion channel expression and activity. J Physiol 594:5861-5867.

Frankland PW, Wang Y, Rosner B, Shimizu T, Balleine BW, Dykens EM, Ornitz EM, Silva AJ (2004) Sensorimotor gating abnormalities in young males with fragile X syndrome and Fmr1-knockout mice. Mol Psychiatry 9:417-425.

Gibson JR, Bartley AF, Hays SA, Huber KM (2008) Imbalance of neocortical excitation and inhibition and altered UP states reflect network hyperexcitability in the mouse model of fragile X syndrome. J Neurophysiol 100:2615-2626.

Goel A, Cantu DA, Guilfoyle J, Chaudhari GR, Newadkar A, Todisco B, de Alba D, Kourdougli N, Schmitt LM, Pedapati E, Erickson CA, Portera-Cailliau C (2018) Impaired perceptual learning in a mouse model of Fragile X syndrome is mediated by parvalbumin neuron dysfunction and is reversible. Nat Neurosci 21:1404-1411.

Goncalves JT, Anstey JE, Golshani P, Portera-Cailliau C (2013) Circuit level defects in the developing neocortex of fragile X mice. Nat Neurosci 16:903-909.

Harris SW, Hessl D, Goodlin-Jones B, Ferranti J, Bacalman S, Barbato I, Tassone F, Hagerman PJ, Herman H, Hagerman RJ (2008) Autism profiles of males with fragile X syndrome. Am J Ment Retard 113:427-438.

He CX, Portera-Cailliau C (2013) The trouble with spines in fragile X syndrome: density, maturity and plasticity. Neuroscience 251:120-128.

Horder J, Wilson CE, Mendez MA, Murphy DG (2014) Autistic traits and abnormal sensory experiences in adults. J Autism Dev Disord 44:1461-1469.

Hu H, Jonas P (2014) A supercritical density of Na(+) channels ensures fast signaling in GABAergic interneuron axons. Nat Neurosci 17:686-693.

Ikuta N, Iwanaga R, Tokunaga A, Nakane H, Tanaka K, Tanaka G (2016) Effectiveness of earmuffs and noise-cancelling headphones for coping with hyper-reactivity to auditory stimuli in children with autism spectrum disorder: a preliminary study. Hong Kong J Occup Ther 28:24-32.

Irwin SA, Patel B, Idupulapati M, Harris JB, Crisostomo RA, Larsen BP, Kooy F, Willems PJ, Cras P, Kozlowski PB, Swain RA, Weiler IJ, Greenough WT (2001) Abnormal dendritic spine characteristics in the temporal and visual cortices of patients with fragile-X syndrome: a quantitative examination. Am J Med Genet 98:161-167.

Jastreboff PJ, Hazell JW (2008) Tinnitus retraining therapy: implementing the neurophysiological model: Cambridge University Press.

Kazdoba TM, Leach PT, Silverman JL, Crawley JN (2014) Modeling fragile X syndrome in the Fmr1 knockout mouse. Intractable Rare Dis Res 3:118-133.

Kern JK, Trivedi MH, Garver CR, Grannemann BD, Andrews AA, Savla JS, Johnson DG, Mehta JA, Schroeder JL (2006) The pattern of sensory processing abnormalities in autism. Autism 10:480-494.

Kim H, Gibboni R, Kirkhart C, Bao S (2013) Impaired critical period plasticity in primary auditory cortex of fragile X model mice. J Neurosci 33:15686-15692.

Knoth IS, Lajnef T, Rigoulot S, Lacourse K, Vannasing P, Michaud JL, Jacquemont S, Major P, Jerbi K, Lippe S (2018) Auditory repetition suppression alterations in relation to cognitive functioning in fragile X syndrome: a combined EEG and machine learning approach. J Neurodev Disord 10:4.

Koeppen J, Nguyen AQ, Nikolakopoulou AM, Garcia M, Hanna S, Woodruff S, Figueroa Z, Obenaus A, Ethell IM (2018) Functional consequences of synapse remodeling following astrocyte-specific regulation of ephrin-B1 in the adult hippocampus. J Neurosci 38:5710-5726.

Kokash J, Alderson EM, Reinhard SM, Crawford CA, Binder DK, Ethell IM, Razak KA (2019) Genetic reduction of MMP-9 in the Fmr1 KO mouse partially rescues prepulse inhibition of acoustic startle response. Brain Res 1719:24-29.

Kotak VC, Takesian AE, MacKenzie PC, Sanes DH (2013) Rescue of inhibitory synapse strength following developmental hearing loss. PLoS One 8:e53438.

Liu XS, Wu H, Krzisch M, Wu X, Graef J, Muffat J, Hnisz D, Li CH, Yuan B, Xu C, Li Y, Vershkov D, Cacace A, Young RA, Jaenisch R (2018) Rescue of fragile X syndrome neurons by DNA methylation editing of the FMR1 gene. Cell 172:979-992 e976.

Lovelace JW, Ethell IM, Binder DK, Razak KA (2018) Translation-relevant EEG phenotypes in a mouse model of fragile X syndrome. Neurobiol Dis 115:39-48.

Lovelace JW, Wen TH, Reinhard S, Hsu MS, Sidhu H, Ethell IM, Binder DK, Razak KA (2016) Matrix metalloproteinase-9 deletion rescues auditory evoked potential habituation deficit in a mouse model of fragile X syndrome. Neurobiol Dis 89:126-135.

Lovelace JW, Rais M, Palacios AR, Shuai XS, Bishay S, Popa O, Pirbhoy PS, Binder DK, Nelson DL, Ethell IM, Razak KA (2019) Deletion of Fmr1 from Forebrain Excitatory Neurons Triggers Abnormal Cellular, EEG, and Behavioral Phenotypes in the Auditory Cortex of a Mouse Model of Fragile X Syndrome. Cereb Cortex. In press

Lucas EK, Jegarl A, Clem RL (2014) Mice lacking TrkB in parvalbumin-positive cells exhibit sexually dimorphic behavioral phenotypes. Behav Brain Res 274:219-225.

Marco EJ, Hinkley LB, Hill SS, Nagarajan SS (2011) Sensory processing in autism: a review of neurophysiologic findings. Pediatr Res 69:48R-54R.

Martin del Campo HN, Measor KR, Razak KA (2012) Parvalbumin immunoreactivity in the auditory cortex of a mouse model of presbycusis. Hear Res 294:31-39.

Miyata S, Kitagawa H (2016) Chondroitin 6-Sulfation Regulates Perineuronal Net Formation by Controlling the Stability of Aggrecan. Neural Plast 2016:1305801.

Mor-Shaked H, Eiges R (2018) Reevaluation of FMR1 hypermethylation timing in fragile X syndrome. Front Mol Neurosci 11:31.

Morris R (2009) Managing sound sensitivity in autism spectrum disorder: new technologies for customized intervention. In: Massachusetts Institute of Technology.

Musumeci SA, Bosco P, Calabrese G, Bakker C, De Sarro GB, Elia M, Ferri R, Oostra BA (2000) Audiogenic seizures susceptibility in transgenic mice with fragile X syndrome. Epilepsia 41:19-23.

Nakahara H, Zhang LI, Merzenich MM (2004) Specialization of primary auditory cortex processing by sound exposure in the "critical period". Proc Natl Acad Sci U S A 101:7170-7174.

Nomura T, Musial TF, Marshall JJ, Zhu Y, Remmers CL, Xu J, Nicholson DA, Contractor A (2017) Delayed maturation of fast-spiking interneurons is rectified by activation of the TrkB receptor in the mouse model of fragile X syndrome. J Neurosci 37:11298-11310.

Olmos-Serrano JL, Corbin JG, Burns MP (2011) The GABA(A) receptor agonist THIP ameliorates specific behavioral deficits in the mouse model of fragile X syndrome. Dev Neurosci 33:395-403.

Oswald AM, Reyes AD (2008) Maturation of intrinsic and synaptic properties of layer 2/3 pyramidal neurons in mouse auditory cortex. J Neurophysiol 99:2998-3008.

Oswald AM, Reyes AD (2011) Development of inhibitory timescales in auditory cortex. Cereb Cortex 21:1351-1361.

Pieretti M, Zhang FP, Fu YH, Warren ST, Oostra BA, Caskey CT, Nelson DL (1991) Absence of expression of the FMR1 gene in fragile X syndrome. Cell 66:817-822.

Pizzorusso T, Medini P, Berardi N, Chierzi S, Fawcett JW, Maffei L (2002) Reactivation of ocular dominance plasticity in the adult visual cortex. Science 298:1248-1251.

Rogers SJ, Wehner DE, Hagerman R (2001) The behavioral phenotype in fragile X: symptoms of autism in very young children with fragile X syndrome, idiopathic autism, and other developmental disorders. J Dev Behav Pediatr 22:409-417.

Rotschafer S, Razak K (2013) Altered auditory processing in a mouse model of fragile X syndrome. Brain Res 1506:12-24.

Roughley PJ, Mort JS (2014) The role of aggrecan in normal and osteoarthritic cartilage. J Exp Orthop 1:8.

Rudelli RD, Brown WT, Wisniewski K, Jenkins EC, Laure-Kamionowska M, Connell F, Wisniewski HM (1985) Adult fragile X syndrome. Clinico-neuropathologic findings. Acta Neuropathol 67:289-295.

Schneider A, Leigh MJ, Adams P, Nanakul R, Chechi T, Olichney J, Hagerman R, Hessl D (2013) Electrocortical changes associated with minocycline treatment in fragile X syndrome. J Psychopharmacol 27:956-963.

Selby L, Zhang C, Sun QQ (2007) Major defects in neocortical GABAergic inhibitory circuits in mice lacking the fragile X mental retardation protein. Neurosci Lett 412:227-232.

Sidhu H, Dansie LE, Hickmott PW, Ethell DW, Ethell IM (2014) Genetic removal of matrix metalloproteinase 9 rescues the symptoms of fragile X syndrome in a mouse model. J Neurosci 34:9867-9879.

Sinclair D, Oranje B, Razak KA, Siegel SJ, Schmid S (2017) Sensory processing in autism spectrum disorders and fragile X syndrome - from the clinic to animal models. Neurosci Biobehav Rev 76:235-253.

Sohal VS, Zhang F, Yizhar O, Deisseroth K (2009) Parvalbumin neurons and gamma rhythms enhance cortical circuit performance. Nature 459:698-702.

Staffend NA, Meisel RL (2011) DiOlistic labeling in fixed brain slices: phenotype, morphology, and dendritic spines. Curr Protoc Neurosci Chapter 2:Unit 2 13.

Takesian AE, Kotak VC, Sanes DH (2012) Age-dependent effect of hearing loss on cortical inhibitory synapse function. J Neurophysiol 107:937-947.

Uutela M, Lindholm J, Louhivuori V, Wei H, Louhivuori LM, Pertovaara A, Akerman K, Castren E, Castren ML (2012) Reduction of BDNF expression in Fmr1 knockout mice

worsens cognitive deficits but improves hyperactivity and sensorimotor deficits. Genes Brain Behav 11:513-523.

Van der Molen MJ, Van der Molen MW, Ridderinkhof KR, Hamel BC, Curfs LM, Ramakers GJ (2012) Auditory and visual cortical activity during selective attention in fragile X syndrome: a cascade of processing deficiencies. Clin Neurophysiol 123:720-729.

Wen TH, Lovelace JW, Ethell IM, Binder DK, Razak KA (2019) Developmental Changes in EEG Phenotypes in a Mouse Model of Fragile X Syndrome. Neuroscience 398:126-143.

Wen TH, Afroz S, Reinhard SM, Palacios AR, Tapia K, Binder DK, Razak KA, Ethell IM (2018) Genetic reduction of matrix metalloproteinase-9 promotes formation of perineuronal nets around parvalbumin-expressing interneurons and normalizes auditory cortex responses in developing Fmr1 knock-out mice. Cereb Cortex:1-14.

Xenos D, Kamceva M, Tomasi S, Cardin JA, Schwartz ML, Vaccarino FM (2018) Loss of TrkB signaling in parvalbumin-expressing basket cells results in network activity disruption and abnormal behavior. Cereb Cortex 28:3399-3413.

Xu H, Kotak VC, Sanes DH (2010) Normal hearing is required for the emergence of long-lasting inhibitory potentiation in cortex. J Neurosci 30:331-341.

Zhang LI, Bao S, Merzenich MM (2001) Persistent and specific influences of early acoustic environments on primary auditory cortex. Nat Neurosci 4:1123-1130.

Zheng K, An JJ, Yang F, Xu W, Xu ZQ, Wu J, Hokfelt TG, Fisahn A, Xu B, Lu B (2011) TrkB signaling in parvalbumin-positive interneurons is critical for gamma-band network synchronization in hippocampus. Proc Natl Acad Sci U S A 108:17201-17206.

Zhou X, Nagarajan N, Mossop BJ, Merzenich MM (2008) Influences of un-modulated acoustic inputs on functional maturation and critical-period plasticity of the primary auditory cortex. Neuroscience 154:390-396.

Zhu X, Wang F, Hu H, Sun X, Kilgard MP, Merzenich MM, Zhou X (2014) Environmental acoustic enrichment promotes recovery from developmentally degraded auditory cortical processing. J Neurosci 34:5406-5415.

Figure legends

Figure 1. Sound evoked event-related potentials (ERPs) in the auditory cortex of AE WT and *Fmr1* KO mice ERPs were evoked by 14 kHz tones (A, C, D, E) or 23 kHz tones (B, F, G, H) in auditory cortex of AE WT and AE *Fmr1* KO (AE WT, n=14 recording sites/6 animals vs AE *Fmr1* KO, n=19 recording sites/8 animals). (A, B) Graphs show average raw ERP traces from all recording sites evoked by 14 kHz (A) or 23 kHz (B) tones in auditory cortex of AE WT and AE *Fmr1* KO mice. (C-H) Quantitative analysis of amplitudes of P1 (C, F), N1 (D, G) and P2 (E, H) ERP responses evoked by 14 Hz (C-E) and 23 Hz (F-H) tones. N1 amplitude of ERP evoked by 14 Hz tone was higher (D, $p<0.05$) in auditory cortex of AE *Fmr1* KO compared to AE WT. No differences were detected in P1, N1 or P2 amplitudes of ERP evoked by 23 Hz tone in auditory cortex of AE *Fmr1* KO compared to AE WT mice. We presented 5 trains of 10 pure tones at 0.25Hz repetition rate. To exclude the effects of habituation, only the responses to the first train (10 responses) were averaged to calculate amplitude and latency of P1, N1 and P2 components. Statistical analysis was done using unpaired t-test: *, $p<0.05$; **, $p<0.01$.

Figure 2. Sound-evoked ERPs in the auditory cortex of SE WT and *Fmr1* KO mice ERPs were evoked by 14 kHz tone (A, C, D, E) and 23 kHz tone (B, F, G, H) in auditory cortex of SE WT and SE *Fmr1* KO (SE WT, n=11 recording sites/5 animals; SE *Fmr1* KO, n=13 recording sites/6 animals). (A, B) Graphs shows average raw ERP traces from all recording sites evoked by 14 kHz (A) or 23 kHz (B) tones (E) in auditory cortex of SE WT and SE *Fmr1* KO mice. (C-H) Quantitative analysis of amplitudes of P1 (C, F), N1 (D, G) and P2 (E, H) ERP responses evoked by 14 Hz (C-E) and 23 Hz (F-H) tones. No differences were detected in P1, N1 or P2 amplitudes

and latencies of ERP evoked by 14 kHz and 23 Hz tones in auditory cortex of SE *Fmr1* KO compared to SE WT mice. Statistical analysis was done using unpaired t-test.

Figure 3. Density of PV cell, but PNNs, is normalized in P21 auditory cortex of SE *Fmr1* KO mice. (A) Confocal image shows PV immunoreactivity and PNN-labeling in auditory cortex of AE WT mice. Scale bar, 250 μm. (B, C) High magnification confocal images show representative examples of PV immunoreactivity and PNN-labeling in AE WT and AE *Fmr1* KO auditory cortex. Scale bar, 50 μm.

(D-I) Quantitative analysis of the density of PV cells (D, G), PNN-containing cells (E, H) and PNN-containing PV cells (F, I) in L2/3 and L4 auditory cortex of AE WT (n=6) and AE *Fmr1* KO (n=5) mice. There was reduced PV cell density in L2/3 (D, AE WT vs AE *Fmr1* KO, $p<0.0001$) and L4 (G, AE WT vs AE *Fmr1* KO, $p<0.0001$) of AE *Fmr1* KO mice compared to AE WT. PNN-containing cell density was lower in L4 of AE *Fmr1* KO mice compared to AE WT (H, AE WT vs AE *Fmr1* KO, $p<0.01$). PNN-containing PV cell density was reduced in L4 of AE *Fmr1* KO compared to AE WT mice (I, AE WT vs AE *Fmr1* KO, $p<0.01$). Statistical analysis was performed using unpaired t-test: **, $p<0.01$; ****, $p<0.0001$.

(J-O) Quantitative analysis of density of PV cells (J, M), PNNs (K, N) and PNN-containing PV cells (L, O) in L2/3 (J-L) and L4 (M-O) of P21 auditory cortex in SE WT and SE *Fmr1* KO mice (SE WT, n=8; SE *Fmr1* KO, n=8). PNN-containing cell density remained lower in L4 of SE *Fmr1* KO mice compared to SE WT (N, $p<0.01$). No differences were observed in the density of PV cells in L2/3 (J) and L4 (M). PNN-containing PV cell density was also similar between SE WT and SE *Fmr1* KO in L2/3 (L) and L4 (O) auditory cortex. Statistical analysis was done using unpaired t-test: **, $p<0.01$.

Figure 4. Analysis of dendritic spine density and morphology in the auditory cortex of AE and SE mice showed beneficial effects of passive sound exposure (A-D) Confocal images showing DiI-labeled dendritic spines in P21 auditory cortex of AE WT (A), AE *Fmr1* KO (B), SE WT (C) and SE *Fmr1* KO (D) mice. Scale bar, 10 μm.

(E, F, I, J) Quantitative analysis of spine density (E, I) and spine morphology (F, J) in L2/3 (E, F) and L5/6 (I, J) auditory cortex of AE WT and AE *Fmr1* KO mice. Spine density was increased in AE *Fmr1* KO mice compared to AE WT in L2/3 (E, AE WT, n=43 dendrites vs AE *Fmr1* KO, n=25 dendrites, $p<0.01$) and in L5/6 (I, AE WT, n=29 dendrites vs AE *Fmr1* KO, n=46 dendrites, $p=0.0090$). No differences in spine morphology were found between AE WT and AE *Fmr1* KO in L2/3 (F) and L5/6 (J). Statistical analysis was done using unpaired t-test (E, I) or two-way ANOVA (for spine volume, F and J): *, $p<0.05$**, $p<0.01$; ****, $p<0.0001$.

(G, H, K, L) Quantitative analysis of spine density (G, K) and spine morphology (H, L) in L2/3 and L5/6 auditory cortex of SE WT and SE *Fmr1* KO mice. There were no differences in spine density between SE *Fmr1* KO and SE WT in L2/3 (G, SE WT, n=23 dendrites vs SE *Fmr1* KO, n=35 dendrites) and L5/6 (K, SE WT, n=47 dendrites vs SE *Fmr1* KO, n=43 dendrites). There were fewer spines with volume $>1\mu^3$ in L2/3 auditory cortex of SE *Fmr1* KO compared to SE WT (H, $p<0.05$). Statistical analysis was done using unpaired t-test (G, K) or two-way ANOVA (for spine volume, H and L): *, $p<0.05$.

Figure 5. Passive sound exposure during development normalized PV protein levels and enhanced TrkB phosphorylation in SE *Fmr1* KO mice. PV protein levels (A-C), total full-length TrkB (D-F), TrkBpY816 (G-I) and TrkBpY515 (J-L) were normalized to β-actin levels in P21 auditory cortex of NE (A, D, G, J), AE (B, E, H, K) and SE (C, F, I, L) WT and *Fmr1* KO

mice. There was reduced PV level in AE *Fmr1* KO compared to AE WT (B, AE WT: n=6 vs AE *Fmr1* KO: n=5, p=0.0403) and no differences were detected in NE (A, NE WT: n =4 vs NE *Fmr1* KO: n=3) and SE *Fmr1* KO (C, SE WT: n=7 vs SE *Fmr1* KO: n=5) compared to their WT counterparts. No differences in total TrkB protein level were found for NE *Fmr1* KO (D, NE WT: n=8 vs NE *Fmr1* KO: n=7), AE *Fmr1* KO (E, AE WT: n=4 vs AE *Fmr1* KO: n=4) and SE *Fmr1* KO (F, SE WT: n=8 vs SE *Fmr1* KO: n=9) compared to their WT counterparts. TrkBpY816 level was decreased in AE *Fmr1* KO compared to AE WT (H, p=0.0479). No differences were detected in SE *Fmr1* KO compared to SE WT (I). TrkBpY515 level was decreased in AE *Fmr1* KO (K, p=0.0306) and increased in SE *Fmr1* KO (L, p=0.0004) compared to their WT counterparts. Statistical analysis was done using unpaired t-test: *, $p<0.05$; ***, $p<0.001$.

Figure 6. Acoustic exposure during early postnatal developmental window restores molecular, cellular and functional alterations observed in the auditory cortex of *Fmr1* KO mice to WT levels. Schematic depiction of the molecular, cellular and functional changes in *Fmr1* KO mice compared to WT mice and the effects of the sound exposure. Left panels, AE *Fmr1* KO mice reared in sound-attenuated environment (AE) during early development showed (1) decreased PV cell density and PV protein levels; (2) increased dendritic spine density; (3) enhanced ERP N1 amplitude; and (4) reduced TrkB phosphorylation on Y816 and Y515 in the auditory cortex compared to WT mice. Right panels, SE *Fmr1* KO mice exposed to 14 Hz tone during development (P9-P21) showed (1) increased PV cell density and PV levels; (2) decreased dendritic spine density; (3) decreased N1 amplitude; and (4) increased phosphorylation of TrkB on Y816 and Y515 in auditory cortex compared to AE *Fmr1* KO mice reared in a sound

attenuated environment. PV levels, spine density and N1 amplitude were not different between SE WT mice and SE *Fmr1* KO mice. Moreover, phosphorylation of TrkB on Y816 and Y515 was respectively similar or higher in auditory cortex of SE *Fmr1* KO mice compared to SE WT mice.

Figure

Click here to download high resolution image

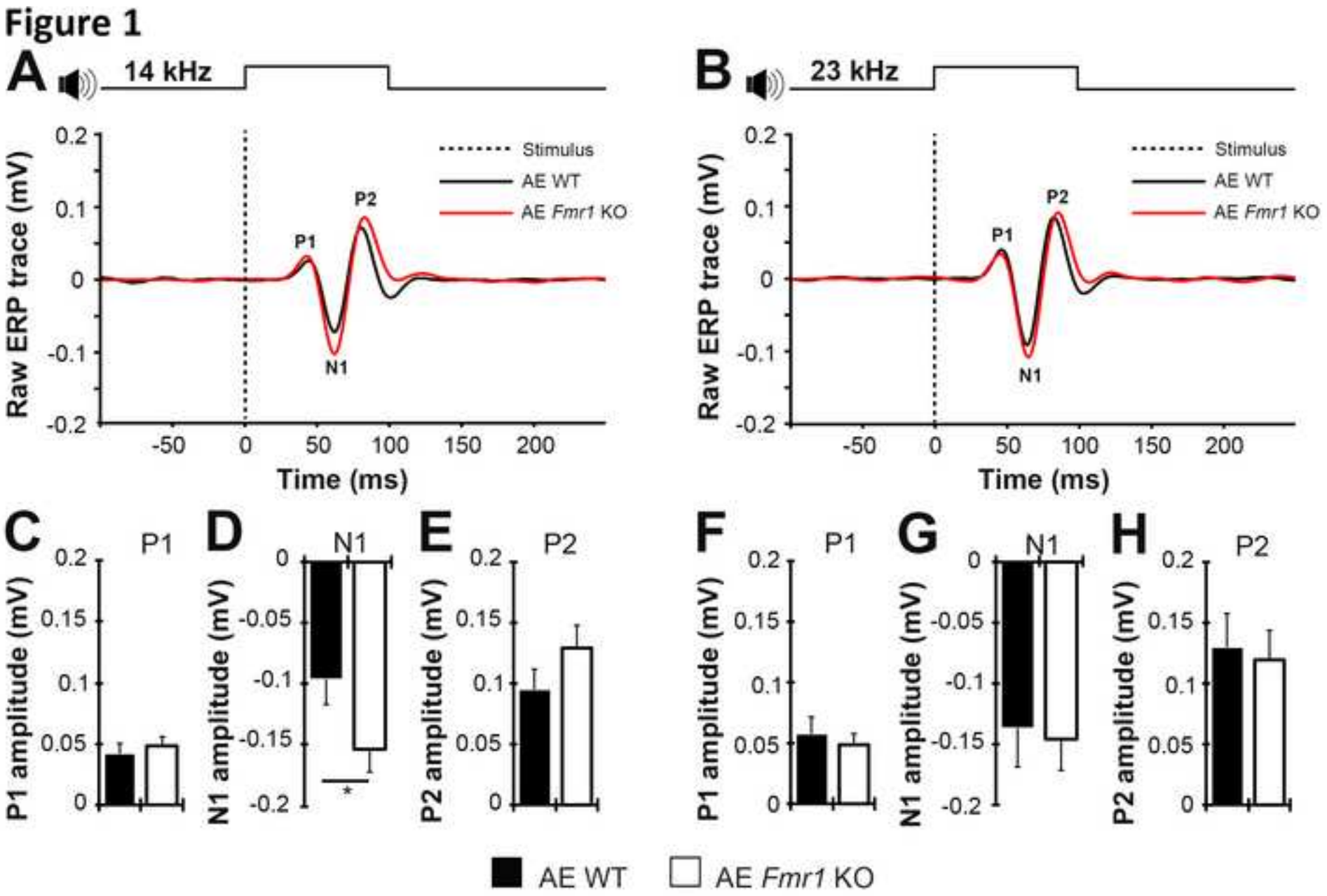

Figure
Click here to download high resolution image

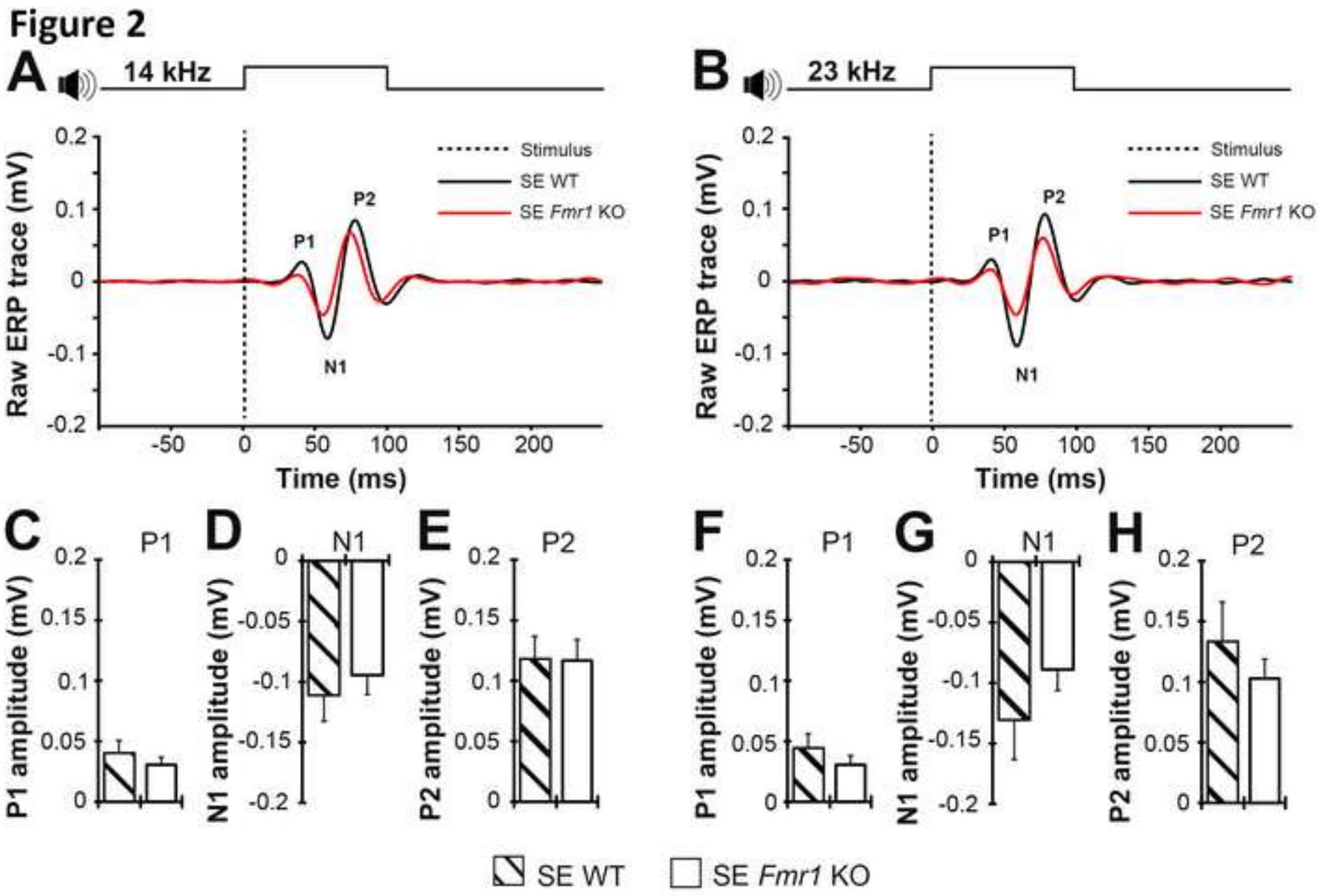

Figure

Click here to download high resolution image

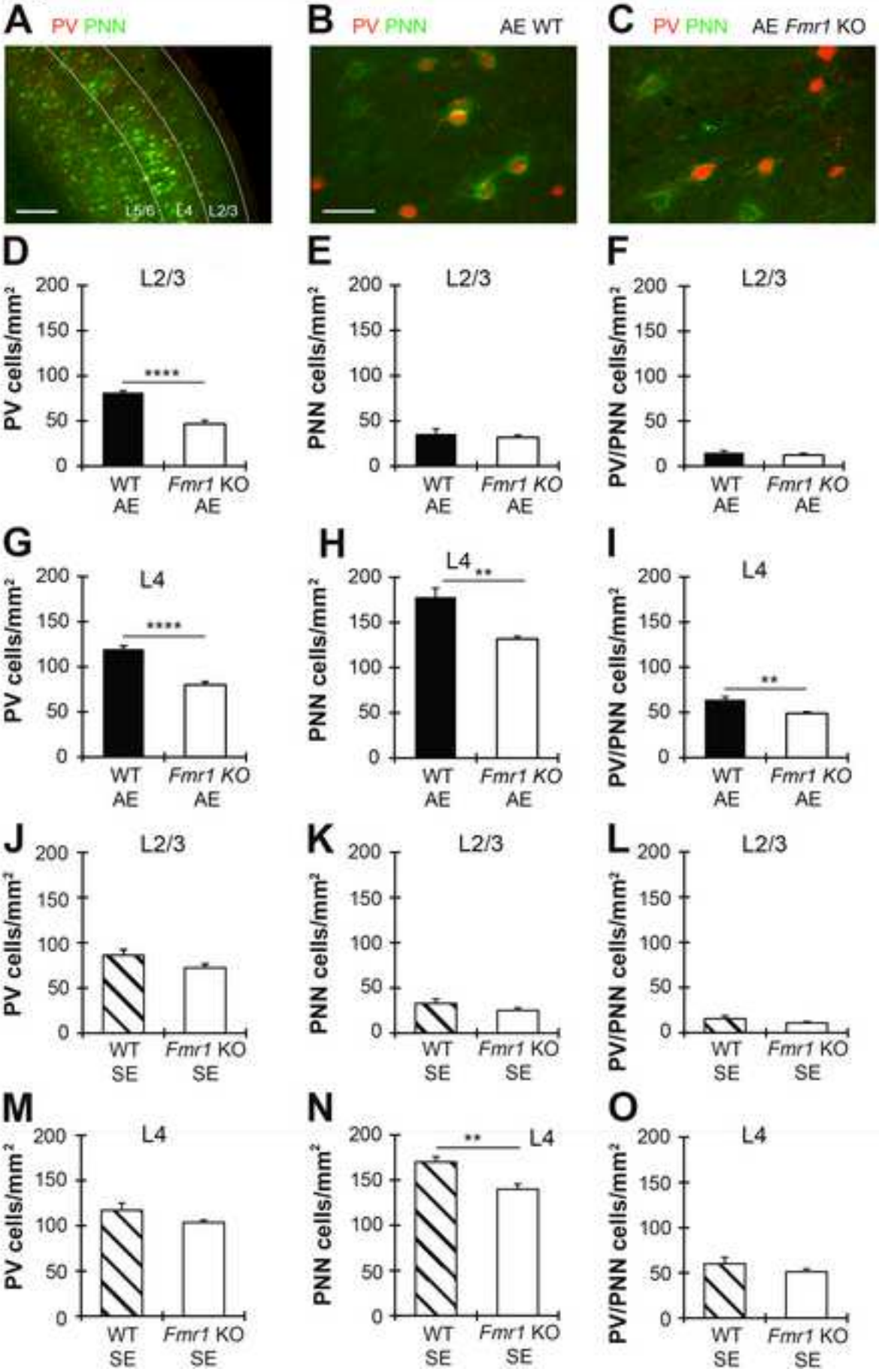

Figure
Click here to download high resolution image

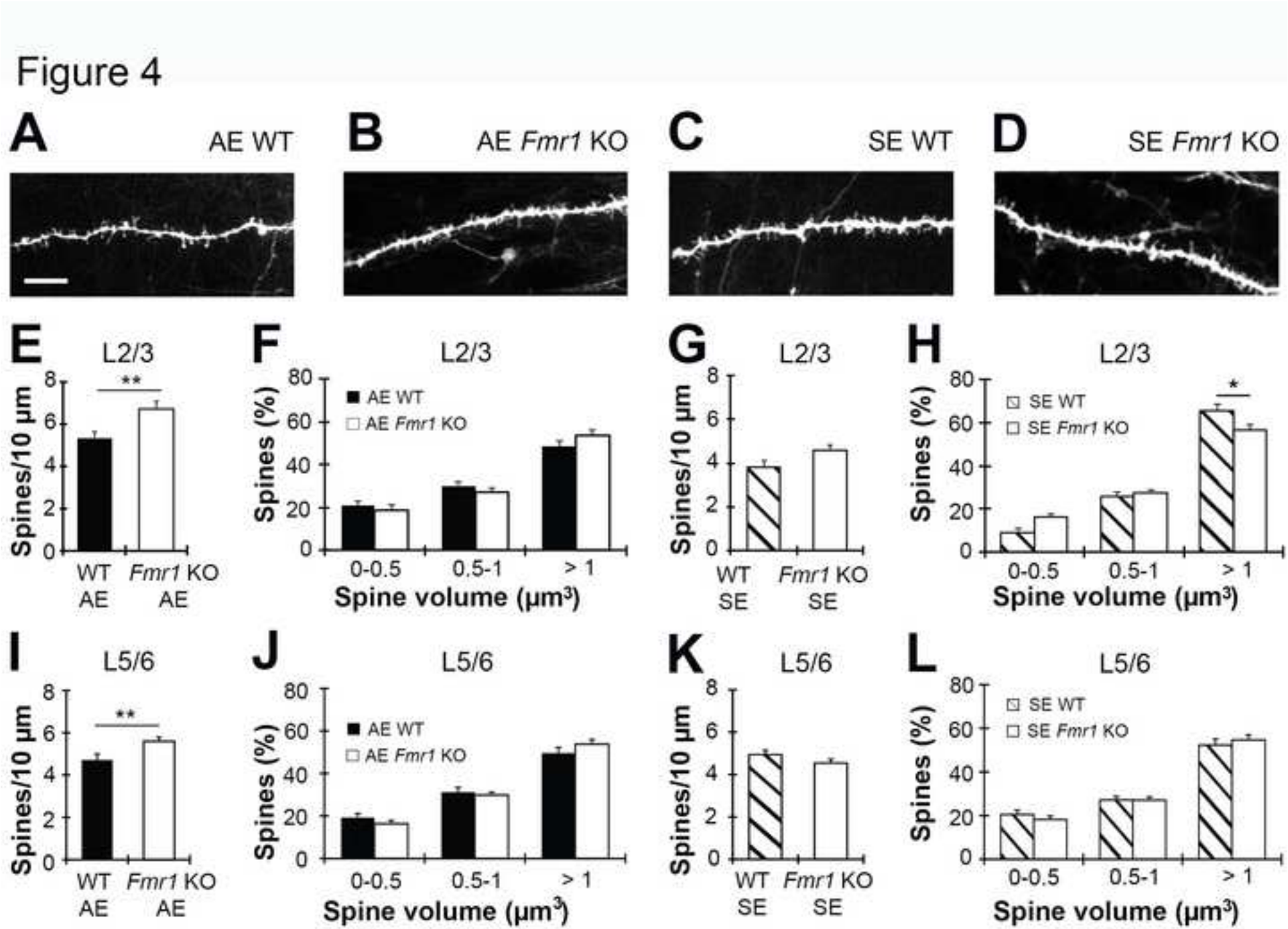

Figure

Click here to download high resolution image

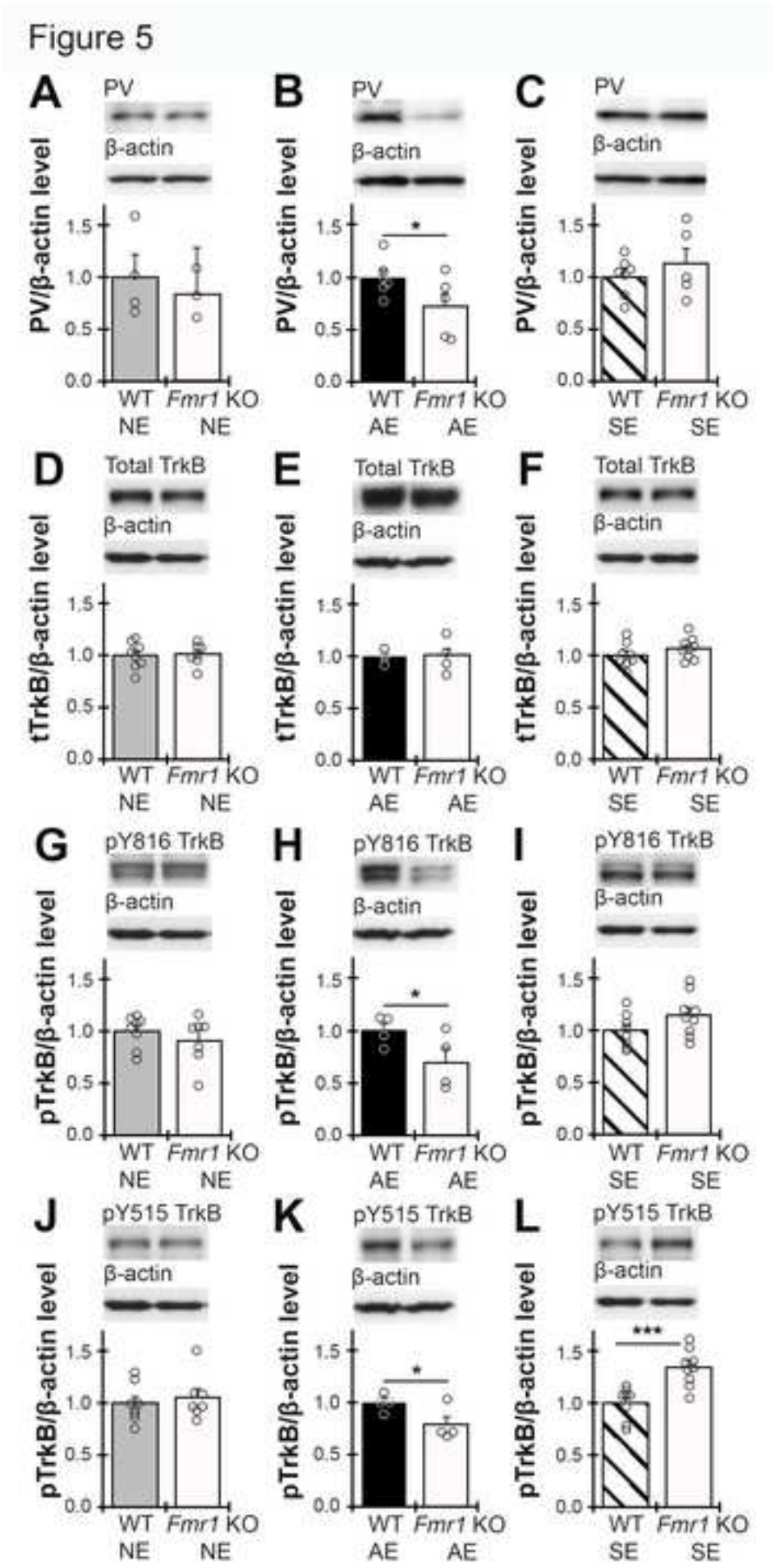

Figure

Click here to download high resolution image

Figure 6

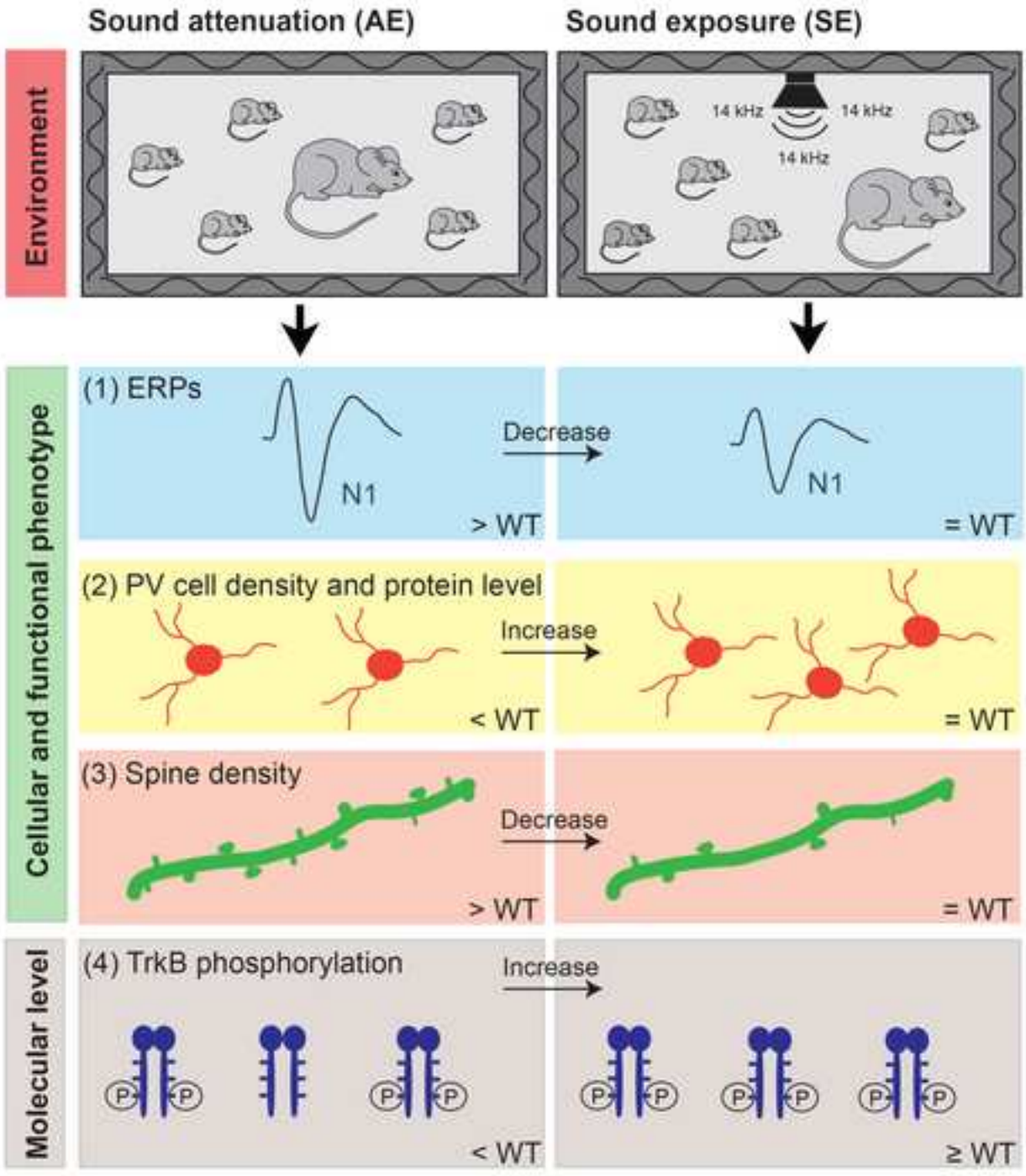

Supplementary Material

Click here to download Supplementary Material: Supplementary_Final_rev_IE.docx

Supplementary Material

Click here to download Supplementary Material: Suppl Figure 1.tif